We are IntechOpen,
the world's leading publisher of
Open Access books
Built by scientists, for scientists

4,800
Open access books available

122,000
International authors and editors

135M
Downloads

Our authors are among the

154
Countries delivered to

TOP 1%
most cited scientists

12.2%
Contributors from top 500 universities

CLARIVATE ANALYTICS
BOOK CITATION INDEX
INDEXED

WEB OF SCIENCE™

Selection of our books indexed in the Book Citation Index
in Web of Science™ Core Collection (BKCI)

Interested in publishing with us?
Contact book.department@intechopen.com

Numbers displayed above are based on latest data collected.
For more information visit www.intechopen.com

A Comparative Thermal Study of Two Permanent Magnets Motors Structures with Interior and Exterior Rotor

Naourez Ben Hadj, Jalila Kaouthar Kammoun,
Mohamed Amine Fakhfakh, Mohamed Chaieb and Rafik Neji
Electrical Engineering Department/ University of Sfax
Tunisia

1. Introduction

Considering the large variety of electric motors, such as asynchronous motors, synchronous motors with variable reluctances, permanent magnets motors with radial or axial flux, the committed firms try to find the best choice of the motor conceived for electric vehicle field.

The electric traction motor is specified by several qualities, such as the flexibility, reliability, cleanliness, facility of maintenance, silence etc. Moreover, it must satisfy several requirements, for example the possession of a high torque and an important efficiency (Zire et al., 2003; Gasc, 2004; Chan., 2004).

In this context, the surface mounted permanent magnets motor (SMPMM) is characterized by a high efficiency, very important torque, and power-to-weight, so it becomes very interesting for electric traction.

In the intension, to ensure the most suitable and judicious choice, we start by an analytical comparative study between two structures of SMPMM which are the permanent magnets synchronous motor with interior rotor (PMSMIR) and the permanent magnets synchronous motor with exterior rotor (PMSMER), then, we implement a methodology of design based on analytical modelling and the electromagnetism laws. Also, in order to understand the thermal behaviour of the motor, we implant a comparative thermal performance of the two structures illustrated with careful attention to the manufacturing techniques used to produce the machine, and the associated thermal resistances and capacitances, to obtain good steady state and transient thermal performance prediction.

2. Modelling of two SMPMM structures

2.1 Structural data

The structures of motors allowing the determination of the studied geometry are based on three relationships.

The ratio β is the relationship between the magnet angular width L_m and the pole-pitch L_p. This relationship is used to adjust the magnet angular width according to the motor pole-pitch.

$$\beta = \frac{L_m}{L_p} \tag{1}$$

$$L_p = \frac{\pi}{p} \tag{2}$$

The ratio R_{ldla} is the relationship between the angular width of a principal tooth and the magnet angular width. This ratio is responsible for the regulation of the principal tooth size which has a strong influence on the electromotive force form.

$$R_{ldla} = \frac{A_{tooth}}{L_m} \tag{3}$$

The R_{did} ratio is the relationship between the angular width of the principal tooth and the angular width of the inserted tooth A_{toothi}. This relationship fixes the inserted tooth size.

$$R_{did} = \frac{A_{tooth}}{L_m} \tag{4}$$

2.2 Geometrical structures of PMSMIR and PMSMER

This part is devoted to an analytical sizing allowing calculation of geometrical sizes of the two SMPMM configurations which are the PMSMER and the PMSMIR.

Figure 1 represents the PMSMER and the PMSMIR with the number of pole pairs is p=4 and a number of principal teeth is 6, between two principal teeth, an inserted tooth is added to improve the wave form and to reduce the leakage flux (Ben Hadj, N. et al., 2007). The slots are right and open in order to facilitate the insertion of coils and to reduce the production cost (Magnussen, F. et al., 2005; Bianchi, N. .et al., 2003; Libert , F. et al., 2004).
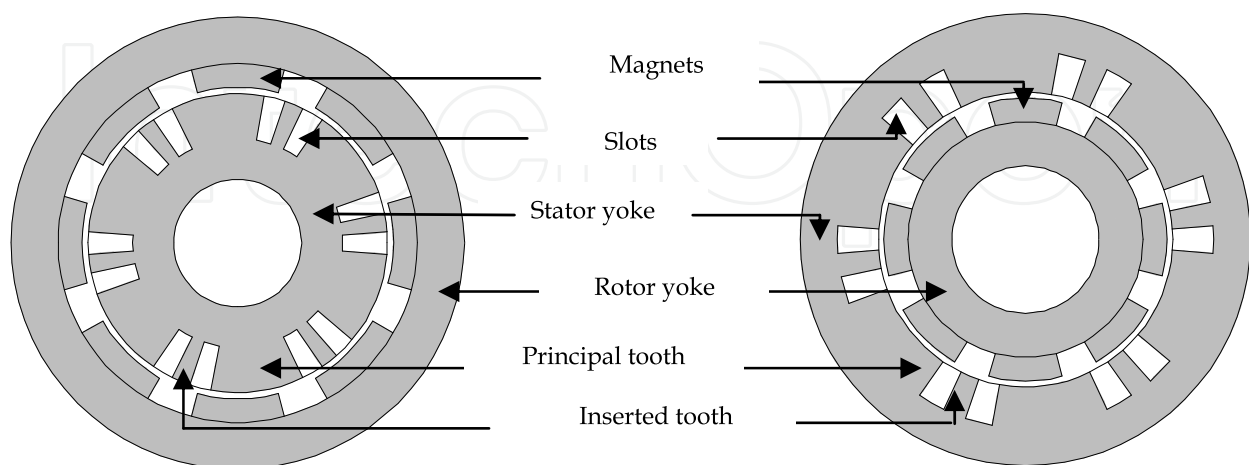

Fig. 1. Permanent magnets motors with exterior rotor and interior rotor

2.3 Analytical sizing of the two SMPMM structures

The analytical study of motor sizing is based on the schedules data conditions parameters (Table 1), the constant characterizing materials (Table 2), the expert data and configurations of the two motors.

Definition	Symbol	Value
Electric vehicle mass	M	1000 kg
Angle of starting	a_d	3°
Time of starting	t_d	4 s
Outside temperature	T_{out}	40°C
Maximum motor power	P_{mmax}	21,635 kW
Winding temperature	T_w	95°C
Base speed of the vehicle	V_b	30 km/h
Maximum Speed of the vehicle	V_{max}	100 km/h
Slots load factor	k_r	0,44
Current density in the slots	δ	7 A/mm²

Table 1. The schedules data conditions

Definition	Symbol	Value
Remanent magnetic induction of the magnets	B_m	1,175 T
Demagnetization Induction	B_c	0,383 T
Magnetic induction in teeth	B_{tooth}	0,9 T
Magnets permeability	μ_a	1,05
Mechanical losses coefficient	k_m	1%
Copper resistivity at 95°C	R_{cu}	17,2 10⁻⁹ Ωm
The copper resistivity variation coefficient	α	0,004
Density of the electrical sheets	M_{vt}	7850 kg
Density of magnets	M_{va}	7400 kg
Density of copper	M_{vc}	8950 kg
Sheets quality coefficient	Q	1,1

Table 2. Specific constants of materials

Expert data

The expert data are practically represented by three sizes which are, the magnetic induction in the air gap B_e, the magnetic induction in the stator yoke B_{sy} and the magnetic induction in the rotor yoke B_{ry}. It should be noted that the zone of variation of these three parameters varies between 0,2 to 1,6T (Ben Hadj et al., 2007).

Structural data

For the two configurations, we adopted the same number of pole pairs P=4, with an air gap thickness equivalent to 2mm, with a relationship β equal to 0,667 and R_{ldla} equal to 1,2.

Data identified by the finite elements method

K_{fu} is the leakage flux coefficient of the PMSMIR which is fixed to 0,95 whereas for the PMSMER, k_{fu} is equal to 0,98. In this context, we define a ratio R_{did} equal to 0,2.

2.4 Geometrical sizes

Geometrical parameters of the two structures motors are defined in figure 2. Where:
1.   The magnet height, h_m
2.   The slots height h_s and the tooth height h_{tooth}
3.   The rotor yoke height, h_{ry}
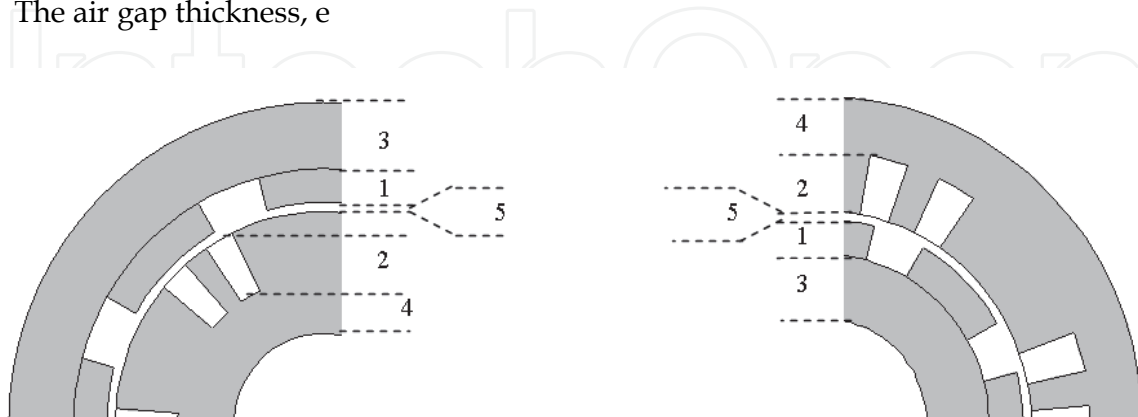4.   The stator yoke height, h_{sy}
5.   The air gap thickness, e

Fig. 2. PMSMER and PMSMIR parameters

In the stator of the PMSMIR, geometrical sizes are defined by:
The slot average width: W_s

$$W_s = \frac{D_m + e + h_{tooth}}{2} A_s \tag{5}$$

The principal tooth section: S_{tooth}

$$S_{tooth} = \frac{D_m + e}{2} A_{tooth} l_m \tag{6}$$

Where l_m, D_m are the average motor length and the average motor diameter.

The inserted tooth section: S_{toothi}

$$S_{toothi} = \frac{D_m + e}{2} A_{toothi} l_m \tag{7}$$

The slot section: S_s

$$S_s = \frac{1}{2} \left[\frac{2\pi}{N_{tooth}} - A_{tooth} - A_{toothi} \right] \frac{D_m + e}{2} l_m \tag{8}$$

In the stator of the PMSMER, geometrical sizes are defined by:
The slot average width: W_s

$$W_s = \frac{D_m - e - h_{tooth}}{2} A_s \tag{9}$$

The principal tooth section: S_{tooth}

$$S_{tooth} = \frac{D_m + e}{2} A_{tooth} l_m \tag{10}$$

The inserted tooth section: S_{toothi}

$$S_{toothi} = \frac{D_m + e}{2} A_{toothi} l_m \tag{11}$$

The slot section: S_s

$$S_s = \frac{1}{2} \left[\frac{2\pi}{N_{tooth}} - A_{tooth} - A_{toothi} \right] \frac{D_m - e}{2} l_m \tag{12}$$

The teeth height h_{tooth} of the PMSMIR and the PMSMER are expressed by equation 13 and 14 where N_{sph} is the number of turns per phase, I_n is the rated current and N_{teeth} in the number of teeth.

$$h_{tooth} = \sqrt{\frac{N_{sph}.I_n}{N_{teeth}\delta K_r A_s} + \left(\frac{Dm + e}{2} \right)^2} - \frac{Dm + e}{2} \tag{13}$$

$$h_{tooth} = \sqrt{\frac{N_{sph}.I_n}{N_{teeth}\delta K_r A_s} + \left(\frac{Dm - e}{2} \right)^2} - \frac{Dm - e}{2} \tag{14}$$

The stator yoke thickness h_{sy} is obtained by the application of the flux conservation theorem, where B_{tooth} is the magnetic induction in the tooth.

$$h_{sy} = \frac{B_{tooth}S_{tooth}}{2l_m B_{sy}} \tag{15}$$

In the rotor of the two structures, geometrical sizes are defined by:
The expression of the magnet height h_m is the same one in the two structures. It is obtained by the application of the Ampere theorem.
Where μ_a is the air permeability and k_{fu} is the flux leakage coefficient.

$$h_m = \frac{\mu_a B_e e}{M(Ta) - \dfrac{B_e}{k_{fu}}} \tag{16}$$

Where the magnet induction $M(Ta)$ at Ta°C is defined by:

$$M(Ta) = M \left[1 + \alpha m (Ta - 20) \right] \tag{17}$$

The rotor yoke thickness h_{ry} is defined:

$$h_{ry} = \frac{B_e S_{tooth}}{2 k_{ful} l_m B_{ry}}$$ (18)

2.5 Electrical sizing

The electromotive force in the two SMPMM structures is expressed by:

$$EMF_i(t) = \frac{8}{\pi} N_{sph} l_m D_m B_e \sin\left(\frac{\pi\beta}{2}\right) \sin\left(\frac{\pi}{2}\beta R_{ldla}\right) \Omega_m \sin(p\Omega_m t)$$ (19)

The motor electric constant : K_e

$$K_e = \frac{12}{\pi} N_{sph} l_m D_m B_e \sin\left(\frac{\pi\beta}{2}\right) \sin\left(\frac{\pi}{2}\beta R_{ldla}\right)$$ (20)

The electromagnetic torque : T_{em}

$$T_{em}(t) = \frac{1}{\Omega} \sum_{i=1}^{3} EMF_i(t)\, i_i(t)$$ (21)

where EMF_i , i_i and Ω_m represent respectively the electromotive force, the current of the i phase and the angular speed of the motor.

The motor rated current I_n is the ratio between the electromagnetic torque and the motor electric constant.

$$I_n = \frac{T_{em}}{K_e}$$ (22)

The phase résistance of the motor : R_{ph}

$$R_{ph} = R_{co}(T_w) \frac{N_{sph} \delta L_{sp}}{I_n / \sqrt{2}}$$ (23)

where $R_{co}(T_w)$ is the copper receptivity at the temperature of winding T_w and L_{sp} is the spire average length (Ben Hadj et al., 2007).

3. Comparative thermal study between the two SMPMM

In this study, the comparison between the two SMPMM structures consists on the thermal analysis which is based upon lumped-circuit analysis. It represents the thermal problems by using the thermal networks, analogous to electrical circuits. The thermal circuit in the steady state consists of thermal resistances and heat sources connected between motor component nodes. For transient analysis, the heat/thermal capacitances are used additionally to take into account the change in internal energy of the body with time. The thermal resistances for conduction and convection can be obtained by:

$$R_{convection} = \frac{l}{Ak} [K/W]$$ (24)

$$R_{conduction} = \frac{l}{A_c h} [K/W] \tag{25}$$

Where l is the distance between the point masses and A is the interface area, k is the heat conductivity, A_c is the cooling cross section between the two regions and h is the convection coefficient calculated from proven empirical dimensionless analysis algorithms.

The heat capacitance is defined as follow:

$$C = V \rho c [Ws/K] \tag{26}$$

Where V is the volume, ρ is the density and c is the heat capacity of the material. The simplified stator for the thermal study of the two SMPMM structure are given by figures 3 and 4, also the thermal model for the two structures are implemented in MATLAB simulater where the different radius for the PMSMER dimensions are defined as follow:

$$R_{carter} = R_1 = R_f + \frac{e}{2} + h_m + h_{ry} + e_{carter} \tag{27}$$

$$R_{rotoryoke} = R_2 = R_f + \frac{e}{2} + h_m + h_{ry} \tag{28}$$

$$R_{magnet} = R_3 = R_f + \frac{e}{2} + h_m \tag{29}$$

$$R_4 = R_f + \frac{e}{2} \tag{30}$$

$$R_{slot} = R_5 = R_f - \frac{e}{2} \tag{31}$$

$$R_{insolator} = R_6 = R_5 - h_s \tag{32}$$

$$R_7 = R_5 - h_s - t_{insolator} \tag{33}$$

$$R_8 = R_7 - h_{sy} \tag{34}$$

The thermal resistances are calculated along the radial direction. The R_i radius are calculated from dimensions of motor, where R_f is the Bore raduis and $t_{insolator}$ is the thickness insulator.

The different radius for the PMSMIR dimensions are defined as follow:

$$R_1 = R_f + \frac{e}{2} \tag{35}$$

$$R_2 = R_f + \frac{e}{2} + h_{tooth} \tag{36}$$

$$R_3 = R_f + \frac{e}{2} + h_{tooth} + t_{insolator} \tag{37}$$

$$R_4 = R_f + \frac{e}{2} + h_{tooth} + t_{isnolator} + h_{sy} \tag{38}$$

$$R_5 = R_f + \frac{e}{2} + h_{tooth} + t_{insolator} + h_{sy} + t_{carter} \tag{39}$$
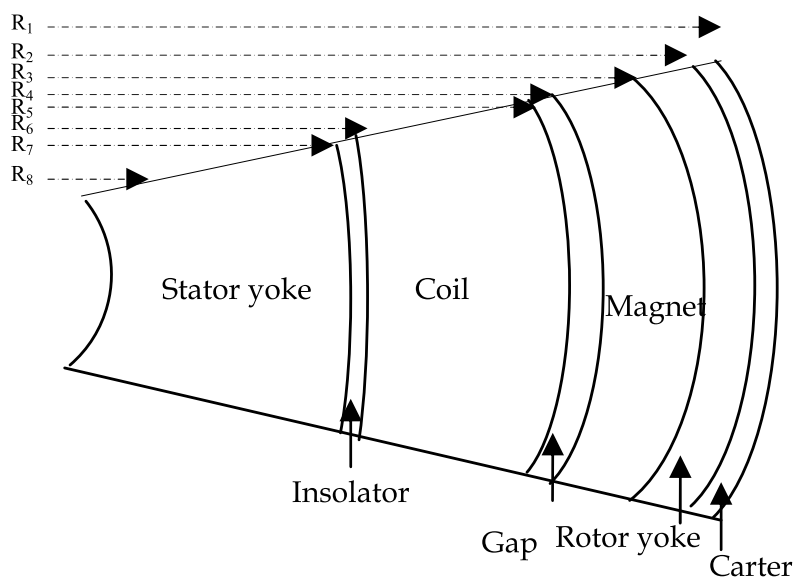

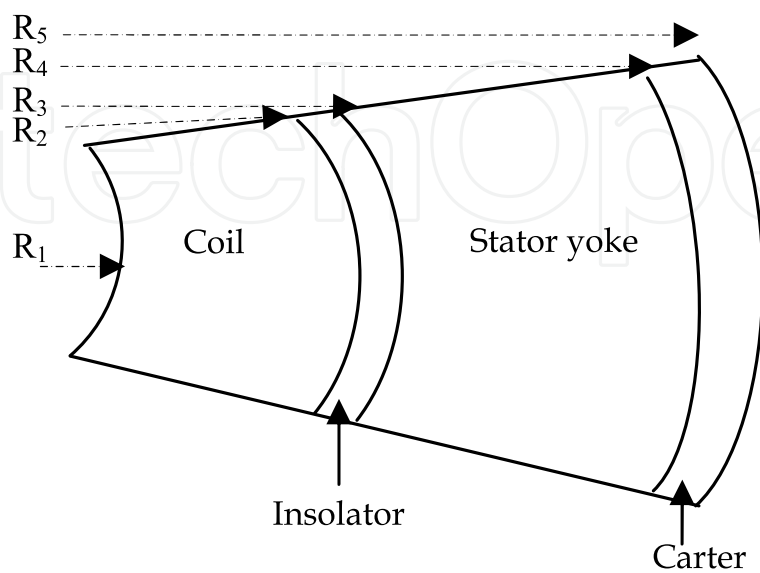Fig. 3. Simplified stator for the thermal study in the PMSMER

Fig. 4. Simplified stator for the thermal study in the PMSMIR

As described earlier, the thermal resistance values are automatically calculated from motor dimensions and material data.

Figure 5 shows the thermal model in transient behaviour of the PMSMIR.
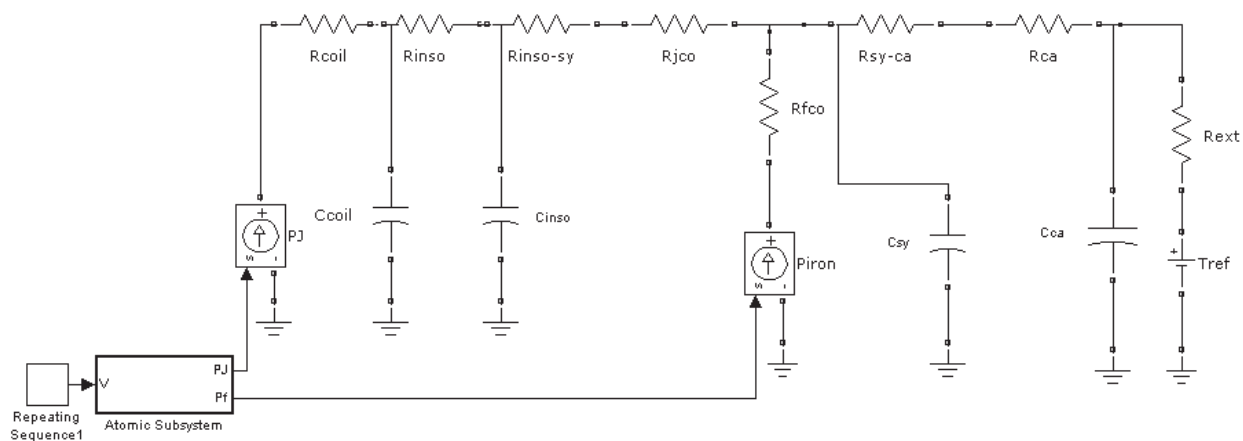
Fig. 5. Thermal model of the PMSMIR in transient behaviour

In this model, the heat sources are respectively the copper losses and iron losses in the stator. The T_i variables are the temperatures in various points of the motor. The expressions of thermal resistances of the PMSMIR result from the resolution of the heat equation at the fields borders.

R_{coil} represents the coil thermal resistance ($K.W^{-1}$).

$$R_{coil} = \frac{1}{4\pi l_m \lambda_{coil}} [1 - 2\frac{R_1^2}{R_2^2 - R_1^2}\ln\frac{R_2}{R_1}] \tag{40}$$

R_{inso} represents the isolator thermal resistance ($K.W^{-1}$).

$$R_{inso} = \frac{\ln\frac{R_3}{R_2}}{2\pi\lambda_{inso}l_m} \tag{41}$$

$R_{inso-sy}$ represents the contact thermal resistance between insolator and the stator yoke ($K.W^{-1}$).

$$R_{inso-sy} = \frac{\frac{1}{300}}{2\pi R_3 l_m} \tag{42}$$

R_{jco} represents the thermal resistance of stator yoke ($K.W^{-1}$).

$$R_{jco} = \frac{\ln\frac{R_4}{R_3}}{2\pi\lambda_{iron}l_m} \tag{43}$$

R_{fco} represents the thermal resistance of conduction in the stator yoke ($K.W^{-1}$).

$$R_{fco} = \frac{1}{4\pi l_m \lambda_{iron}} [1 - 2\frac{R_3^2}{R_4^2 - R_3^2} \ln \frac{R_4}{R_3}] \tag{44}$$

R_{sy-ca} represents the thermal resistance between stator yoke and the carter ($K.W^{-1}$).

$$R_{sy-ca} = \frac{\frac{1}{1500}}{2\pi R_4 l_m} \tag{45}$$

R_{ca} represent the thermal resistance of carter ($K.W^{-1}$).

$$R_{ca} = \frac{\ln \frac{R_5}{R_4}}{2\pi \lambda_{ca} l_m} \tag{46}$$

R_{ext} represents the convection thermal resistance between the carter and ambient air ($K.W^{-1}$).

$$R_{ext} = \frac{l}{hS_{ext}} \tag{47}$$

In the previous expression, S_{ext} represents the outer surface of the motor and h is the heat transfer coefficient between the carter and the ambient air. It can be between 20 and 40 $K.W^{-1}m^{-2}$ for a motor with natural ventilation, and may exceed 80 $K.W^{-1}m^{-2}$ for the motor forced air.

To calculate the outer surface of SMPMM, we considered only the outer surface of the cylinder with radius R_5 and height l_m (Gasc, 2004; Chan., 2004).

$$S_{ext} = 2\pi R_5 l_m \tag{48}$$

The expressions of heat capacities of the PMSMIR are given by the following equations:
C_{coil} represents the heat capacity of coil (JK^{-1}).

$$C_{coil} = \rho_{co} V_{co} C_{th-co} \tag{49}$$

C_{inso} represents the heat capacity of insolator (JK^{-1}).

$$C_{inso} = \rho_{inso} V_{inso} C_{th-inso} \tag{50}$$

C_{sy} represents the heat capacity of stator yoke (JK^{-1}).

$$C_{sy} = \rho_{iron} V_{sy} C_{th-iron} \tag{51}$$

C_{ca} represents the capacity of carter (JK^{-1}).

$$C_{ca} = \rho_{alu} V_{ca} C_{th-alu} \tag{52}$$

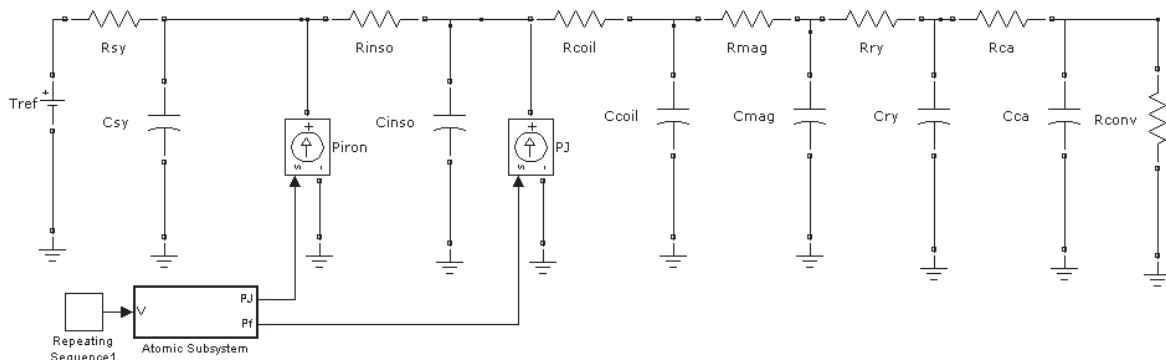Figure 6 shows the thermal model in transient behaviour of the PMSMER.

Fig. 6. Thermal model of the PMSMER in transient behaviour

The expressions of the PMSMER thermal resistances obtained from the resolution of the heat equation at the fields borders.

R_{sy} represents the stator yoke thermal resistance ($K.W^{-1}$).

$$R_{sy} = \frac{1}{4\pi l_m \lambda_{iron}} \left[1 - 2\frac{R_8^2}{R_7^2 - R_8^2} \ln \frac{R_7}{R_8} \right] \tag{53}$$

R_{inso} represents the insolator thermal resistance ($K.W^{-1}$).

$$R_{inso} = \frac{1}{4\pi l_m \lambda_{inso}} \left[2\frac{R_7^2}{R_6^2 - R_7^2} \ln \frac{R_6}{R_7} \right] \tag{54}$$

R_{coil} represents the coil thermal resistance ($K.W^{-1}$).

$$R_{coil} = \frac{1}{4\pi l \lambda_{co}} \left[1 - 2\frac{R_6^2}{R_5^2 - R_6^2} \ln \frac{R_5}{R_6} \right] \tag{55}$$

R_{mag} represents the magnet thermal resistance ($K.W^{-1}$).

$$R_{mag} = \frac{\ln \frac{R_1}{R2}}{2\pi \lambda_{mag} l_m} \tag{56}$$

R_{ry} represents the rotor yoke thermal resistance ($K.W^{-1}$).

$$R_{ry} = \frac{\ln \frac{R_2}{R_3}}{2\pi \lambda_{iron} l_m} \tag{57}$$

R_{ca} represents the thermal resistance of carter. ($K.W^{-1}$)

$$R_{ca} = \frac{\ln \frac{R_1}{R_2}}{2\pi \lambda_{ca} l_m} \tag{58}$$

To calculate the outer surface of SMPMM, we considered only the cylinder outer surface with radius R_1 and the height l_m.

$$S_{ext} = 2\pi R_1 l_m \tag{59}$$

The expressions of heat capacities of the PMSMER are given by the following equations:
C_{mag} represents the heat capacity of magnet (JK^{-1}).

$$C_{mag} = \rho_{mag} V_{mag} C_{th-mag} \tag{60}$$

C_{ry} represents the heat capacity of rotor yoke (JK^{-1}).

$$C_{ry} = \rho_{iron} V_{ry} C_{th-iron} \tag{61}$$

C_{coil} represents the heat capacity of coil (JK^{-1}).

$$C_{coil} = \rho_{co} V_{co} C_{th-co} \tag{62}$$

C_{inso} represents the heat capacity of insolator (JK^{-1}).

$$C_{inso} = \rho_{inso} V_{inso} C_{th-inso} \tag{63}$$

C_{sy} represents the heat capacity of stator yoke (JK^{-1}).

$$C_{sy} = \rho_{iron} V_{sy} C_{th-iron} \tag{64}$$

The below table presents the different thermal conductivities of materials (Jérémi, R., 2003)

Material	Conductivities (Wm-1K-1)	Mass heat capacity (Jkg-1K-1)	Density (Kgm-3)
Copper (Coil)	λ_{co}=5	C_{th-co}= 398	ρ_{co} = 8953
Insolator	λ_{inso} =0.25	$C_{th-inso}$ 1250	ρ_{inso} = 1200
(Iron)Stator Yoke	λ_{iron} =25	$C_{th-iron}$= 460	ρ_{iron} = 7650
Magnet	λ_{mag} =6.5	C_{th-mag}= 420	ρ_{mag} = 7400
aluminium (Carter)	λ_{ca} =180	C_{th-alu} = 883	ρ_{alu} = 2787

Table 3. The thermal conductivities of materials

6. Results and simulations

Simulation results with Matlab software allowed us to obtain the curves of temperatures specific to different materials of the PMSMER and PMSMIR structures. The thermal results at steady and transient state is reached by figures 7, 8.

According to the results, we find that the steady state in the PMSMIR is reached after 4000s. However, the steady state in the PMSMER is achieved after 2000s.

By comparing the results in steady and transient state between the two configurations, we note that temperatures of different parts in PMSMIR are higher than temperatures in PMSMER (especially the coil temperature). That's why, we choose the PMSMER configuration as the best solution in electric traction field.
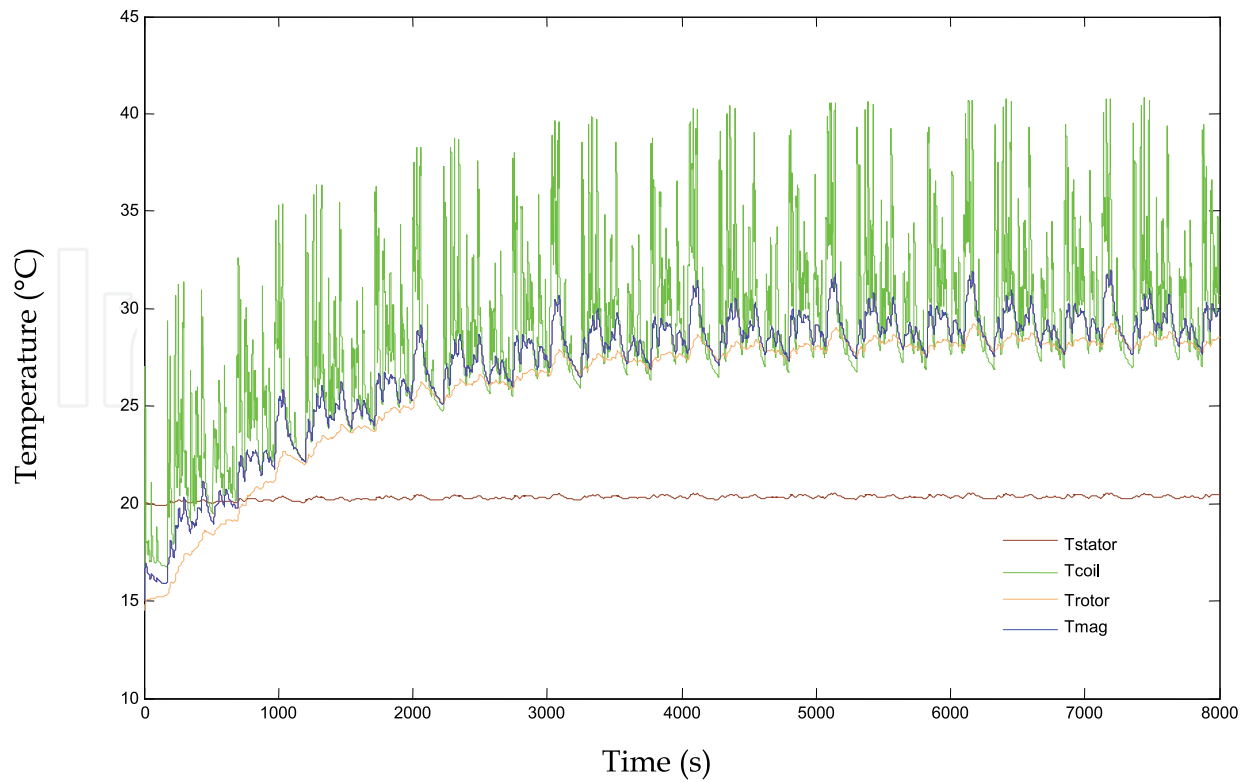
Fig. 7. Various temperatures in different parts of the PMSMER in transient state.
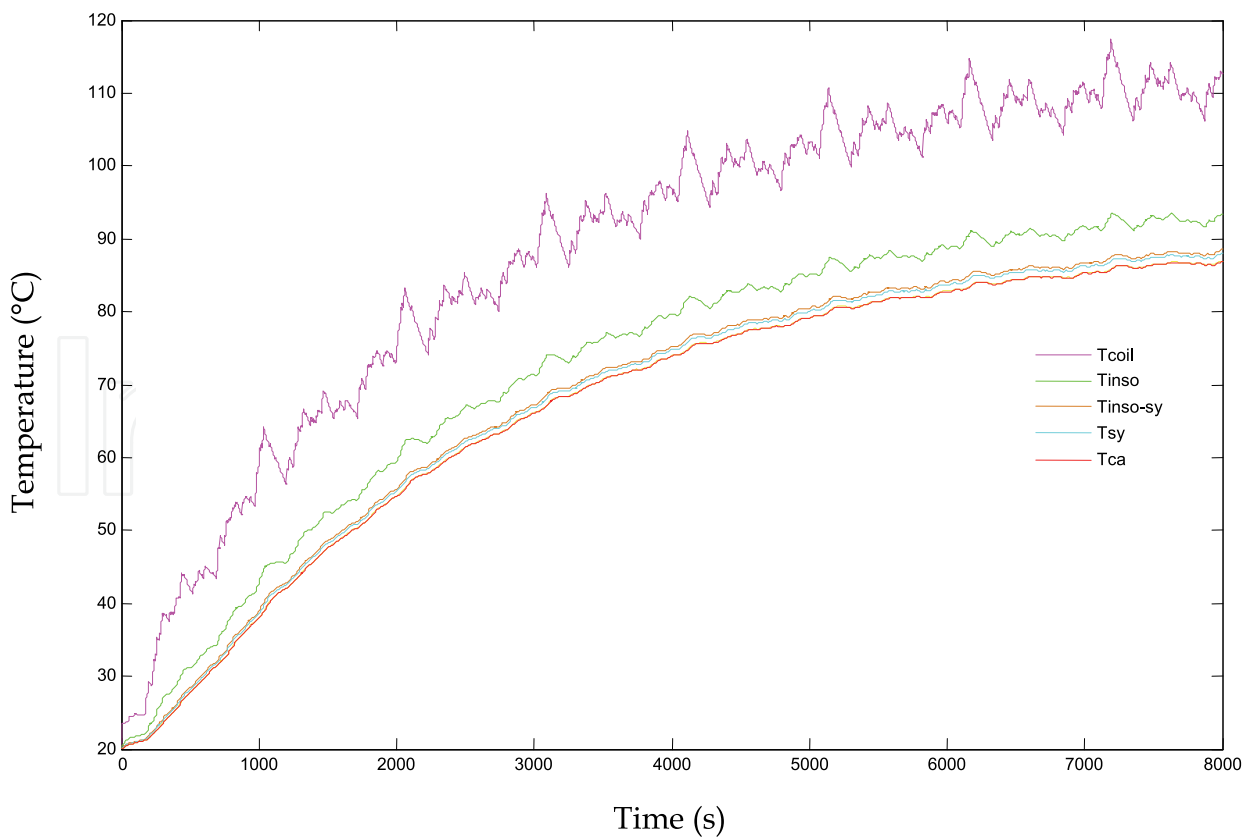

Fig. 8. Various temperatures in different parts of the PMSMIR in transient state.

Moreover, we always look to get a permissible values of coil temperature, based on the proper choice of motors geometric parameters in order to ensure a good compromise between geometric dimensioning and thermal modeling motor.

7. Conclusion

In this paper, a thermal model of two SMPMM with interior rotor and exterior rotor was realised, the intension to compare the evolution of the temperatures of different parts of the two motor configurations and especially the modeling of temperature at the coil is made.

8. References

Chan, C. C. (2004). The Sate of the Art of Electric Vehicles, Journal of Asian Electric Vehicles, Vol. 2, No. 2, pp.579-600.

Junak, J. ; Ombach, G. ; Staton, D. (2008). Permanent Magnet DC Motor Brush Transient Thermal Analysis, 978-1-4244-1736-0/08/$25.00 ©2008 IEEE.

Dorrell David, G. ; Staton Malcolm, A. ; McGilp, I. (2006). Thermal Approach to High Performance Specification, IEEE.

Magnussen, F. ; Lendenmann, H. (2005). Parasitic Effects in PM Machines with Concentrated Windings, IAS 40th Annual Meeting Hong Kong , Volume 2, pp 1045- 1049.

Ben Hadj, N. ; Tounsi, S. ; Neji, R. and Sellami, F. (2007). Real coded Genetic algorithm for permanent magnet motor mass minimization for electric vehicle application, 3rd International Symposium on Computational Intelligence and Intelligent Informatics, Agadir-Morocco, March 28-30, 2007, pp.153-158.

Chin, Y.K.; Nordlund, E.; Staton, E.A. (2003). Thermal analysis – Lumped circuit model and finite element analysis. Sixth International Power Engineering Conference (IPEC), pp. 952- 957.

Staton, D.A. (2001). Thermal analysis of electric motors and generators, Tutorial course at IEEE IAS Annual Meeting, , Chicago, USA .

Holman, J.P. (1992). Heat Transfer, Seventh Edition, McGraw-Hill Publication.

Tounsi, S. (2006). Modélisation et optimisation de la motorisation et de l'autonomie d'un véhicule électrique. Thèse de Doctorat, ENI Sfax

Jérémi, R. (2003). Conception de systèmes hétérogènes en Génie Électrique par optimisation évolutionnaire multicritère, thèse de doctorat, Institut National Polytechnique de Toulouse.

Gasc, L. (2004). Conception d'un actionneur à aimants permanents à faibles ondulations de couple pour assistance de direction automobile Approches par la structure et par la commande, Thèse de doctorat, Institut national Polytechnique de Toulouse.
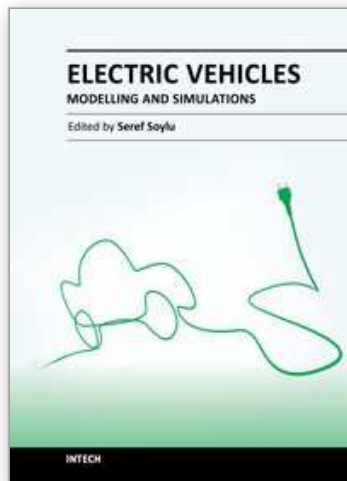
Electric Vehicles - Modelling and Simulations

Edited by Dr. Seref Soylu

In this book, modeling and simulation of electric vehicles and their components have been emphasized chapter by chapter with valuable contribution of many researchers who work on both technical and regulatory sides of the field. Mathematical models for electrical vehicles and their components were introduced and merged together to make this book a guide for industry, academia and policy makers.

How to reference

In order to correctly reference this scholarly work, feel free to copy and paste the following:

Naourez Ben Hadj, Jalila Kaouthar Kammoun, Mohamed Amine Fakhfakh, Mohamed Chaieb and Rafik Neji (2011). A Comparative Thermal Study of Two Permanent Magnets Motors Structures with Interior and Exterior Rotor, Electric Vehicles - Modelling and Simulations, Dr. Seref Soylu (Ed.), ISBN: 978-953-307-477-1, InTech, Available from: http://www.intechopen.com/books/electric-vehicles-modelling-and-simulations/a-comparative-thermal-study-of-two-permanent-magnets-motors-structures-with-interior-and-exterior-ro

INTECH
open science | open minds